

## Article

# Magnetic Structure and Strain State in Fe/V Superlattices Studied by $^{57}\text{Fe}^+$ Emission and Conversion Electron Mössbauer Spectroscopy

Torben E. Mølholt <sup>1,2</sup>, Sveinn Ólafsson <sup>1</sup>, Haraldur P. Gunnlaugsson <sup>1</sup> , Bingcui Qi <sup>1,\*</sup> , Karl Johnston <sup>2</sup> , Roberto Mantovan <sup>3</sup>, Hilary Masenda <sup>4</sup> , Krish Bharuth-Ram <sup>5</sup>, Hafliði P Gíslason <sup>1</sup>, Guido Langouche <sup>6</sup> and Deena Naidoo <sup>4</sup>

<sup>1</sup> Science Institute, University of Iceland, Dunhagi 3, 107 Reykjavík, Iceland; torbenmolholt@gmail.com (T.E.M.); sveinol@hi.is (S.Ó.); hpgunnlaugsson@gmail.com (H.P.G.); hafliði@hi.is (H.P.G.)

<sup>2</sup> Physics Department, ISOLDE, CERN, 1211 Geneva, Switzerland; karl.johnston@cern.ch

<sup>3</sup> CNR-IMM, Unit of Agrate Brianza, Via Olivetti 2, 20864 Agrate Brianza, Italy; roberto.mantovan@mdm.imm.cnr.it

<sup>4</sup> School of Physics, University of the Witwatersrand, Johannesburg 2050, South Africa; hilary.masenda@wits.ac.za (H.M.); deena.naidoo@wits.ac.za (D.N.)

<sup>5</sup> Physics Department, Durban University of Technology, Durban 4000, South Africa; kbharuthram@gmail.com

<sup>6</sup> Instituut voor Kern-en Stralings Fysika, University of Leuven, 3001 Leuven, Belgium; guido.langouche@kuleuven.be

\* Correspondence: bingcui@hi.is



**Citation:** Mølholt, T.E.; Ólafsson, S.; Gunnlaugsson, H.P.; Qi, B.; Johnston, K.; Mantovan, R.; Masenda, H.; Bharuth-Ram, K.; Gíslason, H.P.; Langouche, G.; et al. Magnetic Structure and Strain State in Fe/V Superlattices Studied by  $^{57}\text{Fe}^+$  Emission and Conversion Electron Mössbauer Spectroscopy. *Crystals* **2022**, *12*, 961. <https://doi.org/10.3390/cryst12070961>

Academic Editor: Anton Meden

Received: 19 June 2022

Accepted: 6 July 2022

Published: 10 July 2022

**Publisher's Note:** MDPI stays neutral with regard to jurisdictional claims in published maps and institutional affiliations.



**Copyright:** © 2022 by the authors. Licensee MDPI, Basel, Switzerland. This article is an open access article distributed under the terms and conditions of the Creative Commons Attribution (CC BY) license (<https://creativecommons.org/licenses/by/4.0/>).

**Abstract:** The magnetic properties of the Fe/V superlattices were studied by conventional Conversion Electron Mössbauer Spectroscopy (CEMS) and online  $^{57}\text{Fe}^+$  emission Mössbauer Spectroscopy (eMS) at room temperature (RT) at ISOLDE/CERN. The unique depth-enhanced sensitivity and ultradiluted regime of the probe atoms adopted in this eMS facility enabled the investigation of the magnetic structures and the strain state in the superlattice layers and at the interfaces. The magnetic spectra of the superlattices were found to depend on both the local lattice environment and the strain state of the Fe-lattices. The magnetic polarisation in the V-layers or at the interfaces was not detected at RT. Spectral broadening was evident in the single line component of the eMS due to Fe ions substituted at V-lattice sites in the V-layers of the superlattice, attributable to the lattice strain in the V-layers. Our study demonstrate that with the online eMS technique the effects of the strain state of the superlattice on the magnetic properties of the Fe-layer in the Fe/V multilayer structures can be detected.

**Keywords:** Fe/V superlattices; magnetic properties; strain; Mössbauer Spectroscopy; hyperfine parameters

## 1. Introduction

The magnetic interaction between ferromagnetic layers across a non-magnetic metal spacer layer is of particular interest in application of low-dimensional magnetic systems owing to several interesting phenomena and properties, such as giant magnetoresistance, oscillating interlayer coupling and perpendicular magnetic anisotropy [1–3]. Fe/V superlattices have been a benchmark for various studies on such nanoscale magnetic systems [4–9]. The system shows a great variety of magnetic structures depending on the thickness of the individual Fe- and V-layer, chemical ordering and quality of the interface [4,5,10–12]. Antiferromagnetic interlayer coupling occurs in the Fe/V superlattices with V- and Fe-layer thickness of 13–14 and 2–3 monolayers (MLs), respectively. The presence of atomic mixing during epitaxial growth and other structural defects at Fe/V interfaces may affect the magnetic behavior of Fe atoms depending on a number of the nearest neighboring atoms [13].

Conversion Electron Mössbauer Spectroscopy (CEMS) has been used to study the magnetic properties of the Fe-superlattice systems at the monolayer level enhanced with the  $^{57}\text{Fe}^+$  Mössbauer isotopes [4,5,12,14–16]. It was reported that Fe-layers of thickness  $\leq 5$  MLs were non-magnetic [5]. The magnetic hyperfine profile was found to be significantly different between Fe on V and V on Fe interfaces [12]. However, with CEMS, only the specific Fe-layer and its nearest surrounding neighbour can be probed; only the signal from the Fe-layers in the superlattices contributes the Mössbauer spectrum in this regard. In the present contribution, we applied on-line emission Mössbauer Spectroscopy (eMS) combined with CEMS. The eMS technique probes the whole Fe/V superlattice structure, including the V-layers owing to the large implanting depth of the  $^{57}\text{Mn}^+$  (decays to  $^{57}\text{Fe}^+$ ,  $t_{1/2} = 85.4$  s) beam. Like neutron scattering [17,18], eMS can give additional magnetic information on the V-layers. The isomer shift of the eMS probe which provides a measure of the electron density at the probe nucleus can be linked with the strain variation in the Fe/V interfaces. The unique sensitivity of eMS to the structural changes (e.g., induced by the strain during epitaxial growth and ion implantation) makes possible the study of the effect of the strain on the magnetic properties in and through Fe/V superlattice structures.

## 2. Materials and Methods

The Fe/V superlattices were grown in a custom-built DC magnetron sputtering chamber (Reykjavík, Iceland) on MgO (100) substrates held at 473 K. Base pressure of the chamber was below  $10^{-7}$  Pa. Before sputtering, the MgO substrates were annealed for 30 min at 873 K and targets were pre-sputtered until a stable current was obtained. The Ar gas (99.999% purity) was held at  $3.99 \times 10^{-2}$  Pa during deposition. The deposition rates were  $0.38 \text{ \AA/s}$  and  $0.33 \text{ \AA/s}$  for Fe- and V-layers, respectively, as calibrated using X-ray reflectivity (XRR). A ceramic boron-nitride plate heater was used to heat the sample on the rear side, in the distance from the heater by 7 mm. The applied power on the sputtering target was 70 W, 100 W and 50 W for Fe-, V- and Pd- target, respectively.

The superlattices were grown alternatively with metallic Fe- followed by V-layers under a certain repeating sequence. At room temperature (RT, 300 K), the lattice constants of the body-centred cubic (bcc) structure of Fe, V atoms and the face-centred cubic (fcc) structure of MgO are 0.287 nm, 0.303 nm and 0.421 nm, respectively. Rotating the bcc structures of the Fe and V atoms by  $45^\circ$  with respect to the MgO [100] axis, the lattice mismatches were reduced to  $\sim 4\%$  and  $2\%$  for bcc Fe- and V-layers, respectively [19]. The superlattices are noted as  $X(\text{Fe})/Y(\text{V}) \times Z$ , where X, Y and Z represent the number of MLs of iron and vanadium, and repetition periods, respectively. Four superlattice samples, namely  $16/16 \times 13$ ,  $8/16 \times 13$ ,  $4/16 \times 25$  and  $8/8 \times 25$ , were grown, with a thickness  $\geq 70$  nm for the ion-beam in order to avoid implantation into the MgO substrate during eMS measurements. In addition, a pure V-layer was grown directly on the substrate as a metallic vanadium sample. To prevent superlattices from oxidation, a top Pd layer 3.5 nm thick was deposited on each Fe/V superlattice sample at RT at the end of the growth. Figure 1 gives a schematic of the superlattice structure.

The crystal structures of the superlattices were characterised with X-ray diffraction (XRD) and XRR with a Panalytical X'pert diffractometer (Cu K $\alpha$  radiation wavelength of 0.15406 nm) mounted with a hybrid monochromator/mirror on the incident side and a  $0.27^\circ$  collimator on the diffraction side (Eindhoven, Netherlands). XRD scans were measured for the superlattice Fe/V (200) in high-angle region ( $50^\circ$ – $75^\circ$ ). Low angle XRR measurements were used to calibrate the growth rate of individual layer and then to characterize the quality of the superlattice structure.

$^{57}\text{Fe}^+$  eMS was performed at the ISOLDE facility at CERN (Geneva, Switzerland) following implantation of radioactive  $^{57}\text{Mn}^+$  ( $t_{1/2} = 85.4$  s) through  $\beta$ -decay to  $^{57}\text{Fe}^+$  ( $t_{1/2} = 140$  ns) 14.4 keV gamma rays. Beams of  $^{57}\text{Mn}^+$  ions were produced by 1.4 GeV proton-induced fission of uranium in a heated UCx target and element selective extraction using multi-photon laser ionization [20]. After acceleration to 50 keV and through the magnetic mass separation, a pure beam of  $2 \times 10^8$   $^{57}\text{Mn}^+$  /s was obtained and implanted

at RT into the sample held in a vacuum chamber ( $\sim 10^{-4}$  Pa), at an incident angle ( $\theta_I$ ) of  $30^\circ$  relative to the surface normal of the sample. The maximum implantation fluence is ca.  $1 \times 10^{12}$   $^{57}\text{Mn}^+/\text{cm}^2$ ,  $<10^{-3}$  at.% to ensure the dilute concentration regime and avoid overlapping damage cascades. The eMS spectra were recorded using a parallel plate resonance detector containing enriched  $^{57}\text{Fe}^+$  stainless steel electrodes. The intrinsic line-shape of the detector was a Voigt profile with Lorentzian broadening of  $\Gamma_{Det.} = 0.29$  mm/s and Gaussian broadening of  $\sigma_{Det.} = 0.08$  mm/s. The detector was mounted  $90^\circ$  relative to the beam. This gives an emission angle  $\theta_E = 90^\circ - \theta_I = 60^\circ$  (relative to the surface normal of the sample). The  $8/8 \times 25$  sample was measured additionally at  $\theta_E = 0^\circ$  where the sample was rotated after implantation and measured during the decay of  $^{57}\text{Mn}^+$ . Each spectrum was constantly recorded for several minutes with sufficient statistics needed for the fitting procedures.

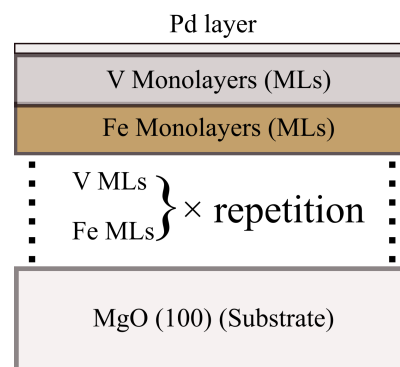


**Figure 1.** Schematic layout of the superlattice structure of the sample. The repetition is for the period of the number of V and Fe monolayers (Fe MLs/V MLs  $\times$  repetition).

CEMS measurement was performed at RT by mounting the sample in a parallel plate avalanche detector filled with acetone gas at 2500 Pa and applied voltage set at  $\sim 1$  kV [21] (intrinsic Voigt line-shape of this detector has  $\Gamma_{Det.}$  of 0.10 mm/s and  $\sigma_{Det.}$  of 0.05 mm/s). Samples were measured at an emission angle  $\theta_E = 0^\circ$  (with the sample surface normal facing the source). The  $16/16 \times 13$  sample was measured additionally at  $\theta_E = 45^\circ$ .

Velocities and isomer shifts are calibrated relative to  $\alpha$ -Fe at RT. Note that the velocity scale of the eMS spectra (usually inverted relative to CEMS spectra) has been interchanged to allow a direct visual comparison with the CEMS spectra in this paper. The spectra were analysed by a simultaneous fitting method using the analysis code Vinda [22].

### 3. Results and Analysis

Figure 2 shows representative XRR low-angle (a) and XRD high-angle (b) spectra of the  $8/16 \times 13$  sample, which proves the good single crystalline structure and the interface quality achieved [4].

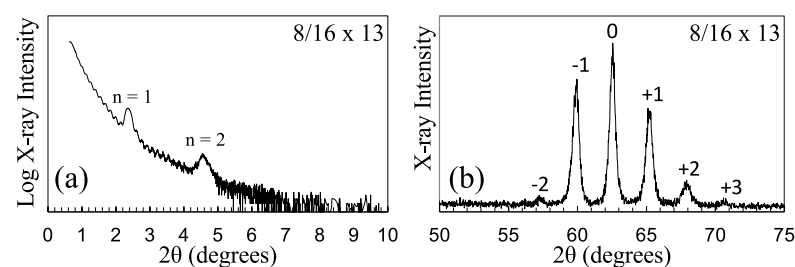


**Figure 2.** (a) XRR low-angle specular X-ray diffraction of the  $8/16 \times 13$  Fe/V superlattice. Two superlattice satellites are observed at  $2\theta = 5^\circ$ . (b) High angle XRD of the same sample shows [200] single crystalline superlattice peaks.

Simulation of the XRR low-angle spectra gave an interface quality or roughness of  $\pm 2$  ML for all the Fe/V superlattices. The broadened second order superlattice peak as compared to the first order peak in XRR spectrum ( $n = 2$  and  $1$  see Figure 1) suggests that the superlattices have an improved interface sharpness and a reduced inter-diffusion. Interface diffusions in the Fe/V superlattices would have caused the second and the first order superlattice peaks to have the similar full width at half maximum [23]. With a more precise local probe in eMS, the interface structure and the magnetic properties of the Fe/V superlattices can be further investigated based on the hyperfine magnetic field distribution.

Figure 3 shows the RT (300 K)  $^{57}\text{Fe}^+$  CEMS spectra of the Fe/V superlattice samples measured at two different emission angles. As the CEMS probes only the Fe-layers in the Fe/V-lattices, the CEMS spectra exhibit clearly magnetically split sextet patterns for the superlattices with 8 and 16 ML Fe layers.

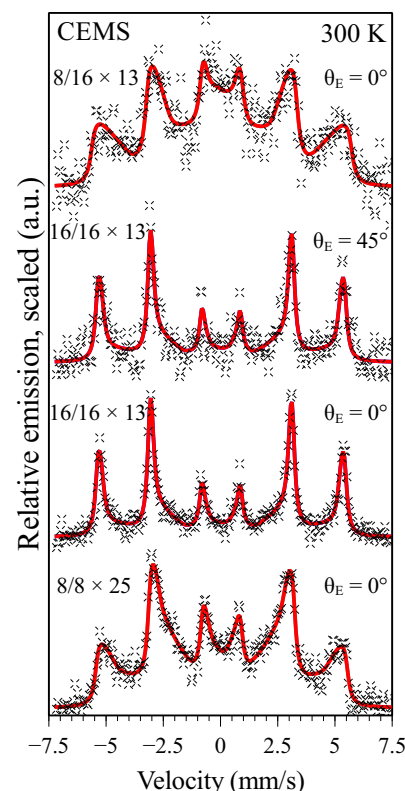


**Figure 3.**  $^{57}\text{Fe}^+$  CEMS spectra of the Fe/V superlattices at 300 K. The emission angles ( $\theta_E$ ) relative to the sample surface normal are indicated.

Figure 4 shows the RT (300 K)  $^{57}\text{Fe}^+$  eMS spectra of the Fe/V superlattices and the pure vanadium samples measured at two different emission angles. As compared to CEMS, the eMS is more depth-sensitive and can probe through the whole Fe/V superlattice structures, including V-layers. Therefore, the eMS spectra are additionally dominant with a single peak, similar to the pure vanadium sample, which shows only a single peak and non-magnetic.

The eMS spectra were therefore analysed with multi-components: magnetic sextet splitting lines assigned to  $^{57}\text{Fe}^+$  ions implanted in the Fe-lattice layers ( $\text{Fe}_{Fe}$ ) similar to the CEMS spectra in Figure 3, a single Voigt line-shape assigned to  $^{57}\text{Fe}^+$  ions implanted in the V-lattice layers ( $\text{Fe}_V$ ) and a small single line contribution from Fe implanted into the Pd layer ( $\text{Fe}_{Pd}$ ) (based on the isomer shift  $\delta = 0.1715$  mm/s according to [24], with a fixed area fraction of 2.0 % expected from the stopping of the  $^{57}\text{Mn}^+ / ^{57}\text{Fe}^+$  in that layer according to SRIM calculations [25]). The  $\text{Fe}_{Fe}$  component is not fully symmetric, similar to the observation reported by Kalska et al. [12]. This feature can be described with a linear coupling between the isomer shift ( $\delta$ , central position of a resonance) and the magnetic

hyperfine field ( $B_{hf}$ , sextet splitting of the resonance lines), namely magnetic hyperfine field distribution (MHFD) function [22] as shown in Equation (1).

$$\delta_{Fe_{Fe}} = \delta_{Fe_{Fe}(33T)} + \delta_1 \times (B_{hf} - 33T) \quad (1)$$

where  $\delta_{Fe_{Fe}}$  and  $B_{hf}$  refer to the centroid shift and the magnetic hyperfine field of the sextet feature ( $Fe_{Fe}$  component).  $\delta_{Fe_{Fe}(33T)}$  refers to the isomer shift of the sextet line from the central Fe-layer (without any V neighbours), which would be bulk-like with  $B_{hf} = 33$  T.  $\delta_1$  is the coupling parameter. The item 33 T is the magnetic hyperfine field of bulk  $\alpha$ -Fe. The coupling between magnetic hyperfine field and isomer shift shows that the isomer shift depends on the location of the Fe atoms in the Fe-lattice layer.

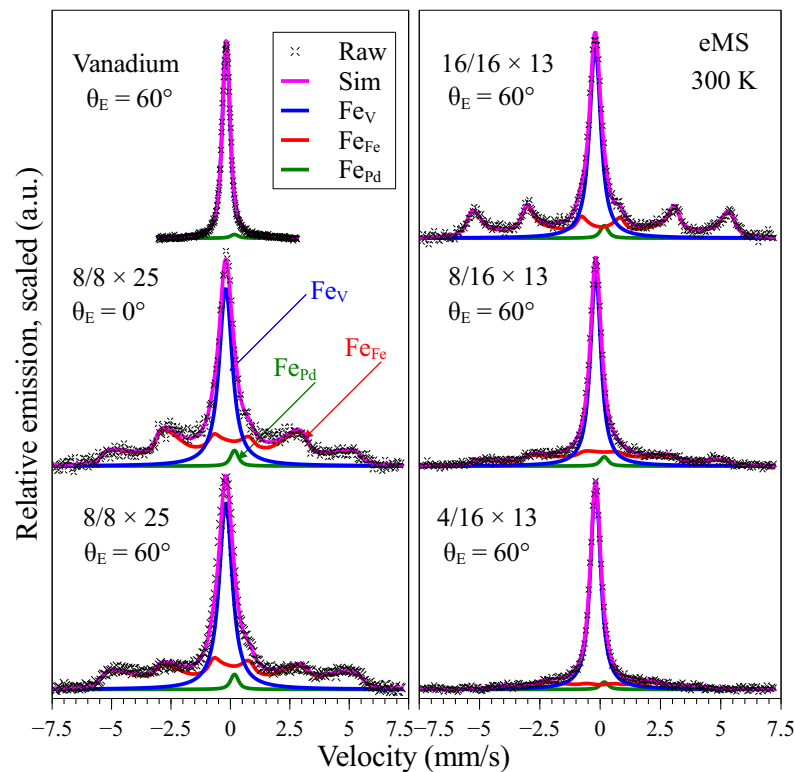


**Figure 4.**  $^{57}Fe^+$  eMS spectra of the Fe/V superlattices and the pure vanadium sample at 300 K. Emission angles ( $\theta_E$ ) relative to the sample surface normal are indicated.

The eMS and CEMS spectra were then simultaneously analysed with MHFD the function with Equation (1) and Voigt line profile. The extracted hyperfine parameters and spectral areas are summarized in Table 1. The hyperfine field distributions of the spectra are shown in Figure 5.

Figure 5 shows that the hyperfine field distribution is dependent on the superlattice structure. The  $B_{hf}$  from CEMS is generally higher than that from eMS. The penetration depth of the  $^{57}Mn^+$  beam in the Fe/V superlattices in this study was estimated to be  $\sim 400$  Å with a peak concentration at  $\sim 200$  Å by the code SRIM [25]. The  $^{57}Fe^+$  probe ions in eMS passing through the Fe- or V-layers would also stop at the Fe/V interface. Therefore, with the CEMS probing only the Fe-layers, and the eMS probing through the whole Fe/V superlattice structures, the  $B_{hf}$  measured by the eMS would be attenuated and more distributed when compared with the CEMS. Thus, the eMS contains the information of both V-layers and the Fe/V interfaces.

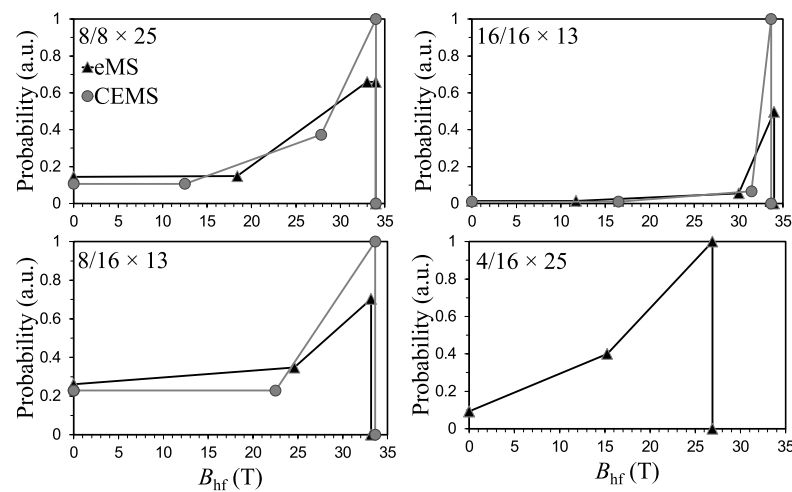


**Figure 5.** The normalized magnetic hyperfine field distributions (MHFD) from the analyses of eMS (triangles) and CEMS (circles) spectra.

**Table 1.** The extracted room temperature (RT) fitting parameters of the spectra in Figures 3 and 4.  $\langle B_{hf} \rangle$  and  $\langle \delta_{Fe_{Fe}} \rangle$  are the average magnetic hyperfine fields and centroid shifts of the sextet patterns, respectively;  $\delta_1$  is the coupling constant in MHFD function;  $\delta$  and  $\sigma$  are the isomer shift and the Gaussian broadening (with the detector line-width  $\sigma = 0.08$  mm/s subtracted and Lorentzian width set to the natural line-width  $\Gamma = 0.29$  mm/s) of the single line component ( $Fe_V$ , i.e., substitutional Fe in V-lattice layer); and A is the relative area fraction of the component. (Note: the parameters for  $Fe_{Pd}$  are fixed and not listed).

Sample	Method	$Fe_{Fe}$ (Fe in Fe-Layer, MHFD)				$Fe_V$ (Fe in V-Layer, Single Line)		
		$\langle B_{hf} \rangle$ (T)	$\langle \delta_{Fe_{Fe}} \rangle$ (mm/s)	$\delta_1$ (mm/s)	A (%)	$\delta$ (mm/s)	$\sigma$ (mm/s)	A (%)
8/8 × 25	CEMS	23.9(9)	0.01(3)	0.0037(9)	100(2)	-	-	-
	eMS	22.4(9)	0.01(3)	0.0037(9)	57(2)	−0.196(4)	0.31(2)	41(2)
16/16 × 13	CEMS	28.7(2)	0.01(6)	0.003(2)	100(6)	-	-	-
	eMS	26(3)	0.01(6)	0.003(2)	52(5)	−0.206(3)	0.189(3)	46(1)
8/16 × 13	CEMS	21(2)	0.03(5)	0.002(2)	100(5)	-	-	-
	eMS	19(3)	0.02(5)	0.002(2)	39(2)	−0.184(4)	0.15(2)	58(2)
4/16 × 25	eMS	17(4)	0.00(5)	0.001(2)	22(2)	−0.190(3)	0.149(5)	75(2)
Vanadium	eMS	-	-	-	-	−0.178(2)	0.000(3)	98(1) *

\* The numbers in parentheses represent the  $1\sigma$  error in the last digit.

#### 4. Discussion

To further test the assignment of the  $Fe_V$  component to the substitutional Fe in the V-layers in the eMS measurements, we compare the measured and the calculated area fractions of the  $Fe_V$  component by taking into account the stoichiometry of the superlattice, implantation range and recoil free fractions ( $f$ -factors calculated using the Debye model for the reported Debye temperatures,  $\Theta_D$ ) of the  $^{57}Fe^+$  atoms in the superlattice structure. According to the SRIM calculations [25], more  $^{57}Mn^+$  come to rest in the Fe-layers (4–8% depending on the stoichiometry) due to a higher stopping probability of  $^{57}Mn^+$  in the Fe-layers compared to the V-layers. The Debye temperatures of Fe in V-layers ( $\Theta_D = 390$  K [26,27]) and in Fe-layers ( $\Theta_D = 460$  K [28]) were adopted in the mass defect approximation [29]. Figure 6 shows the plot of the calculated versus the measured area fraction of the  $Fe_V$  component in different superlattice structures.

The linear relationship in Figure 6 supports that the  $\text{Fe}_V$  signal originates only from the substitutional Fe atoms in V-layers. The  $\text{Fe}_{Fe}$  component originates entirely from the Fe-layers. This is also supported by the eMS of the pure metallic vanadium sample, which is non-magnetic, as shown in Figure 4 and Table 1.

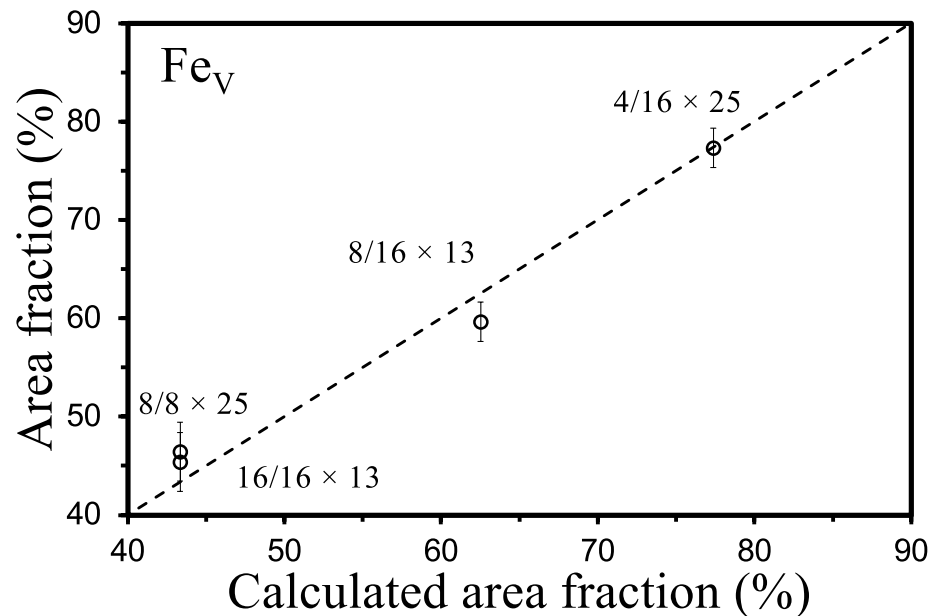


**Figure 6.** Plot of the calculated (horizontal) versus the measured (by eMS, vertical) area fraction of the  $\text{Fe}_V$  component in different superlattice structures (the dotted line represents the calculated, the unfitted circles represent the measured area fraction of the superlattice as indicated).

Table 2 gives the line intensity ratio of the sextet components for the superlattices measured at different emission angles ( $\theta_E$ ). The results show that for all the superlattices, at the emission angle  $\theta_E = 0^\circ$ , (i.e., with emission of  $\gamma$ -ray perpendicular to magnetic field), the line intensity ratio follows 3:4:1, and only changes with  $\theta_E$  different from  $0^\circ$ . This indicates that the magnetic hyperfine fields are in the sample plane and perpendicular to the  $\gamma$ -ray direction [15]. A striking exception is that for the  $8/16 \times 13$  sample, the line intensity ratio follows a ratio of 3:3.2:1 (at  $\theta_E = 0^\circ$ ) and 3:2.5:1 (at  $\theta_E = 60^\circ$ ). This indicates the Fe-layer in this sample has deviated from the single crystalline bcc structure and is in a textured structure. The texture feature of the Fe-layers would create multi-domain magnetic structures in the superlattice. This sample has lower Fe/V ratio and total thickness, and is more prone to intermixing of Fe with V atoms at the interface and more strain build up in the Fe-layers by the neighbouring V-layers in the superlattice. Both could weaken the magnetic hyperfine field of the Fe-layers in the superlattice.

**Table 2.** The line intensity ratio of the sextet component measured at different emission angles ( $\theta_E$ ), i.e., the angle between the principal axis of the electric field gradient tensor (sample surface normal) and the gamma emission direction.

$\theta_E$	Method	Sample			
		$8/8 \times 25$	$8/16 \times 13$	$16/16 \times 13$	$4/16 \times 25$
$0^\circ$	CEMS	3:4:1	3:3.2:1	3:3.9:1	-*
	eMS	3:4:1	-	-	-
$45^\circ$	CEMS	-	-	3:3.7:1	-
$60^\circ$	eMS	3:2:1	3:2.5:1	3:2.5:1	-

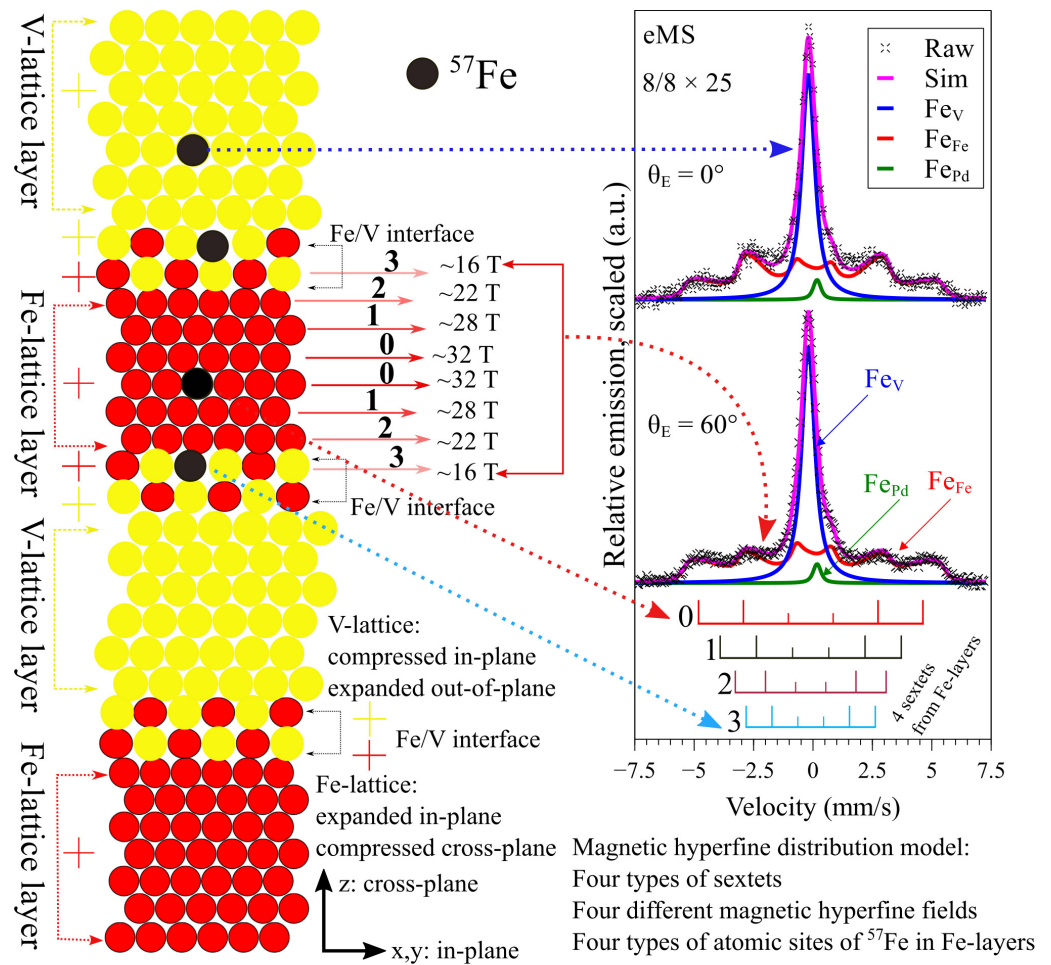
\* it has not been detected.

The magnetic hyperfine field in Figure 5 shows a broad distribution and varies with the Fe/V ratio and the number of the Fe-layers in the superlattice. One or two distinct high fields can be solved in the samples with the Fe-layers  $\geq 8$  ML and correlated with the Fe atoms with zero, one or two V atoms as the nearest neighbours in the superlattice. The  $4/16 \times 25$  sample has the lowest number of Fe-layers (4 MLs), which are barely enough to form a clear sextet-like pattern (Figure 4) and the maximum  $B_{hf}$  value is only  $\sim 27$  T, lower than the magnetic hyperfine field of bulk  $\alpha$ -Fe ( $\sim 33$  T). According to the results reported in [30], for every Fe atom as the nearest and next nearest neighbour to the central Fe in a single-phase bcc structure of Fe-V alloys, that is replaced by V, the Fe hyperfine field in the alloy is suppressed approximately by 3 T. This confirms there is an interdiffusion of Fe and V atoms at the interface of about 1–2 ML in the Fe/V superlattices grown for this study. For the superlattices with 8 ML and 16 ML of Fe atoms, the resolved highest hyperfine field is above 30 T. The  $16/16 \times 13$  sample has the highest number of Fe-layers (16 MLs), which exhibits a strong sextet-like MHFD pattern (Figures 3 and 4) and a maximum hyperfine field of  $B_{hf} > 33$  T (the value expected for the bulk  $\alpha$ -Fe, see Figure 5). This agrees with the results reported in [12], which can be interpreted as: (a) the interlayer ferromagnetic exchange interaction in the Fe-layer is weaker when the non-magnetic spacer V layer is thicker; (b) the intralayer ferromagnetic exchange interaction is weaker when the magnetic layer (Fe-layer) is thinner.

Different MHFDs are observed between the CEMS and eMS for the same sample. Generally, a lower average magnetic hyperfine field  $\langle B_{hf} \rangle$  was measured in eMS than that in CEMS. This is probably due to an extra ion-beam-induced intermixing of Fe and V atoms at the interface during the eMS measurements which is absent in CEMS measurements. Such a mixing can reduce the magnetic hyperfine field  $\langle B_{hf} \rangle$  of the central Fe-layers in the superlattice. This was observed in Fe/Zr multilayer [31,32] with CEMS, where much higher fluences (up to  $4 \times 10^{17}$  protons/cm<sup>2</sup> and  $2 \times 10^{16}$  Ar/cm<sup>2</sup>) than this study ( $< 10^{12}$  <sup>57</sup>Mn/cm<sup>2</sup>) were applied; the sextet-like component was greatly reduced and disappeared at the highest fluence.

In the eMS measurements, the final location of the implanted probe atoms in the superlattice is practically random. The probe atoms can end up in the V-layers, next to the Fe-layer (interfaces) or deep within the Fe-layers. The magnetic hyperfine field distributions are thus the superpositions of several distributions mainly from the interface layer and the next layer but also from the layers further into the superlattice (intralayer).

Figure 7 schematically illustrates the interdiffusion, structure and angle-dependent magnetic hyperfine field distribution of the  $8/8 \times 25$  superlattice sample. At the interface there is possibly 1–2 monolayer intermixing of Fe and V atoms. Owing to the different lattice size of Fe and V atoms in bcc structure, in-plane lattices are expanded in Fe-layer and compressed in V-layers; and cross-plane lattices are compressed in Fe-layers and expanded in V-layer. As a result, the Fe-lattice volume increases, and the V-lattice volume decreases in the Fe/V superlattices as compared to the Fe- and V-lattice volumes in bulk bcc structure. In the most extreme case, the lattice mismatch between the Fe- and V-layers would result in a 5–6% distortion ( $a/c$ ) of the bcc lattices at the Fe/V interface in the superlattices. Consequently, the lattice strain is built up in the Fe- and V- lattice layer and the misfit dislocations are created at the Fe/V interface to relax the strain with increasing thickness of the Fe- or V-layer [33]. The thicker the layer, the more the strain is relaxed, the less the magnetic hyperfine field is affected/reduced. Therefore, the central Fe-lattice layer has the highest magnetic hyperfine field which decreases towards the Fe/V interface. The additional intermixing of Fe and V atoms due to the recoil of Fe probe atoms at and close to the Fe/V interface can also induce lattice disorder around the interface layer and cause a lower magnetic hyperfine field in eMS measurement than that in CEMS. This also agrees with the variation of the magnetic hyperfine field strength with the number of the Fe MLs in the superlattice structure.



## Fe/V superlattice: 8/8 x 25

## eMS analysis

**Figure 7.** Schematic showing that the distribution of magnetic hyperfine field is related to the local lattice environments of the  $^{57}\text{Fe}^+$  probe atoms in the Fe/V superlattice structure, with 8/8 × 25 sample as an example, which contains 25 periods of evenly spaced 8/8 Fe/V superlattices.

According to the variation of the magnetic hyperfine field with the location of the Fe atoms with respect to the interface, the profile of the individual magnetic hyperfine field of the  $\text{Fe}_{Fe}$  component could be described. Fe probe atoms in the central Fe-ML give rise to the highest magnetic hyperfine field (probes fully surrounded by the Fe atoms). As it moves towards the Fe/V interface, the magnetic hyperfine field decreases and the Fe probe atoms at the interface surrounded by both the V and Fe atoms as the nearest neighbours give rise to the lowest magnetic hyperfine field. The Fe probe atoms surrounded fully by the V atoms exhibit no magnetic field splitting, but a single line in the eMS.

The isomer-shift of bulk Fe is 0 mm/s (from definition). However, the isomer shift of the  $\text{Fe}_{Fe}$  component is found to depend slightly on the superlattice structure (Figure 4 and Table 1). This can be qualitatively explained by two main contributions: (i) lattice strain and (ii) neighbour effect.

- (i) The lattice strain (relative to the unperturbed  $\alpha$ -Fe-lattice) gives rise to a non-zero isomer shift of the  $\text{Fe}_{Fe}$  component ( $\delta_{\text{Fe}_{Fe}}$ ) [34–36]. There is a lattice misfit of ~5 % between  $\alpha$ -Fe and V atoms at the Fe/V interface (the in-plane lattice constant is 0.287 nm for Fe, and 0.303 nm for V). This would create an in-plane compressive strain for V-lattices and tensile strain for Fe-lattices, leading to a body-centred tetragonal (bct) structure at the interface. This strain state in the superlattice structure depends on the thickness of each lattice layer and formation

- of misfit dislocations at the interface. In-plane lattice parameters are expanded for Fe-layers and compressed for V-layers; on the other hand, cross-plane lattice parameters are contracted for Fe-layers and expanded for V-layers, respectively. The Fe-lattice volume therefore increases, and the V-lattice volume decreases in the superlattice [37]. The change in lattice volume will likewise change the electron density and isomer shift of the implanted  $^{57}\text{Fe}^+$  probe atoms in the lattice layers.
- (ii) The isomer shift of  $\text{Fe}_{Fe}$  depends on the type of neighbours around the probe atom, and this is defined as the neighbour effect ( $\delta_N$ ). This effect arises from the different electronic configurations of Fe and V atoms. It depends on the relative amount of either element in the neighbourhood of the Fe probe atom. In the simplest case, the neighbour effect can be parameterized as:

$$\delta_N = \alpha_V \times \delta_{FeV} + (1 - \alpha_V) \times \delta_{FeFe} \quad (2)$$

where  $\alpha_V$  is the relative number of V atoms (0 to 1) in the neighbourhood of the Fe probe atoms.  $\delta_{FeV}$  and  $\delta_{FeFe}$  are the isomer shifts of Fe atoms in the V-layer and in the Fe-layer, respectively, neglecting the strain effects.  $\delta_{FeFe} = 0$  by the definition of the zero isomer shift of Fe in  $\alpha$ -Fe (bulk-like Fe without strain).

The observed isomer shift  $\delta_{Obs}$  measured from the superlattice is then modelled as:

$$\delta_{Obs} = \delta_S + \delta_N = \delta_S + \alpha_V \times \delta_{FeV} \quad (3)$$

$\delta_S$  can be treated as constant throughout the superlattice free of lattice dislocations.  $\delta_N$  can vary depending on the relative locations of the Fe probe atoms in the superlattices.

In the central Fe-layer which shows the highest saturated magnetic hyperfine field, the neighbour effect is minimal ( $\delta_N \sim 0$ ); only the strain ( $\delta_S$ ) contributes to the changes of the isomer shift. The centroid shift of the magnetic hyperfine field from the central Fe-layer (corresponding to  $B_{hf} = 33$  T) should therefore give a good estimation on the  $\delta_S$  value, i.e.,  $\delta_{Fe,center} = \delta_{FeFe}(33 \text{ T}) = \delta_S$ . Figure 8 compares the isomer shifts of the  $\text{Fe}_{Fe}$  component from the central Fe-layer ( $\delta_{FeFe}(33 \text{ T})$ ) in the superlattice samples analysed with the MHFD function with the literature data obtained from the Fe-foils subjected to high pressures [35,36].

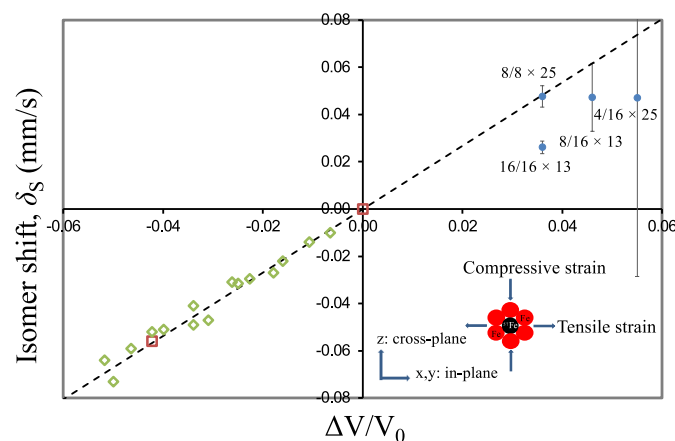


**Figure 8.** The influence of strain on the isomer shift ( $\delta_S$ ) of the Fe-layer. Blue dots represent the isomer shifts of the  $\text{Fe}_{Fe}$  component from the central Fe-layers ( $\delta_S = \delta_{Fe,center}$ ) in the superlattice sample as indicated, where the neighbour effect is negligible, only the strain effect is valid. The related error bars are added to each data series. The literature data obtained from the compressed Fe-foils are plotted for comparison.  $\Delta V/V_0$  stands for the volume change of the Fe-lattice layer. The dashed line is defined by  $\Delta \delta_S / \Delta(\Delta V/V_0) = 1.34$  mm/s adapted with permission from [36]. Red squares represent the data adapted with permission from [36] and green diamonds the data adapted with permission from [35] using the  $(\Delta V/V_0)/\Delta P = 5.95 \times 10^{-4}$  kbar $^{-1}$  conversion adapted with permission from [36]. Copyrighted by the American Physical Society. Negative (positive) sign of  $\Delta V/V_0$  indicates a compression (an expansion) of the Fe-lattice layer.

For the  $4/16 \times 25$  sample, the isomer shift of the central Fe-layer ( $\delta_S = \delta_{Fe.Centre}$ ) was obtained by extrapolation to  $B_{hf} = 33$  T in the fitting analysis of the eMS with the MHFD function. A large error bar at this extrapolated data point is due to the low fraction of the  $Fe_{Fe}$  component (lowest Fe/V ratio) in this sample. A negative  $\Delta V/V_0$  indicates a compression and a positive  $\Delta V/V_0$  expansion of the Fe-lattice (cross-plane) layer as compared to the bulk  $\alpha$ -Fe. The dotted line follows the trend observed by Pipkorn et al. [36] and Southwell et al. [35] from the metallic Fe-layers under high pressure. The linear plot in Figure 8 indicates that the isomer shift decreases linearly with the compression of the Fe-lattice in the superlattice. The data from the  $8/8 \times 25$  sample follows the trend of the literature data, while the data from the  $16/16 \times 13$  sample obviously deviates from the trend, and the value of strain in this sample cannot be deduced. However, based on the isomer shift measured for this sample, if the same linear trend is assumed, this sample should be less strained as compared to the  $8/8 \times 25$  sample. The strain-related isomer shifts of the  $4/16 \times 25$ ,  $8/16 \times 13$  and  $8/8 \times 25$  samples are comparable. Based on the linear trend in Figure 8, this indicates that the Fe-layers in these superlattices should experience similar amount of strain. This is expected; during the epitaxy growth of the Fe/V superlattice, the energy will be created owing to the build-up strain and increases as the layer grows. When the layer thickness reaches a critical value (the strain build-up energy reaches the highest point), a high density of misfit dislocations will form at the interface to release the strain for the final layer. This suggests that the strain build-up has reached the maximum at the Fe-layer thickness of 8 ML. The Fe-layer in  $16/16 \times 13$  sample has reached the critical thickness and has already released most of the strain at the final growth, as compared to the  $8/8 \times 25$  sample. As for the  $8/8 \times 25$  sample, both the Fe- and V-layer are not thick enough to reach the critical thickness to release the strain. The Fe-lattice and V-lattice layers are coherently aligned and still fully strained in this sample. The data for the  $8/16 \times 25$  and the  $4/16 \times 25$  samples seem to support this observation but are more difficult to interpret due to large errors, probably owing to lower number Fe-layers in these two samples.

At the Fe/V interface,  $\alpha_V = 1/2$ ,  $B_{hf} \sim 0$  T. According to Equation (3), there is:

$$\delta_{Fe_V} = 2(\delta_{Obs}(0\text{ T}) - \delta_S) \quad (4)$$

$\delta_{Obs}(0\text{ T})$  is the isomer shift of the  $Fe_{Fe}$  component extrapolated to  $B_{hf} = 0$  T in the eMS analysed with the MHFD function. Therefore, we can also estimate the isomer shift of the  $Fe_V$  component ( $\delta_{Fe_V}$ ) with Equation (4), using the  $\delta_S = \delta_{Fe.Centre}$  value determined in Figure 8 for each superlattice sample.

The neighbour effect can be estimated from the isomer shift of the  $Fe_V$  component by assuming that only the interface atoms are affected by the neighbour effect; the isomer shift at the interface  $\delta_{Fe_V,V}$  can be expressed as:

$$\delta_{Fe_V,V} = (\delta_{Obs} - \delta_S) \left( \frac{N_V}{N_V - 1} \right) \quad (5)$$

where  $N_V$  is the number of V-layers in the superlattice. Using  $\delta_S = \delta_{Fe.Centre}$  found for the  $Fe_{Fe}$  component in Fe-layer (Figure 8), and  $\delta_{Obs} = \delta_{Fe_V}$  measured from the eMS spectra, based on Equation (5), one gets  $\delta_{V,V} = -0.262(2)$  mm/s for the  $8/8 \times 25$  sample. This value is comparable to the isomer shift of the  $Fe_V$  component  $\delta_{Fe_V} = -0.21(3)$  mm/s estimated with Equation (4) for the same sample and the value  $\delta_V = -0.237$  mm/s inferred from the data of Ingalls et al. [34] at  $\Delta V/V_0 = -0.05$  (fully strained Fe/V superlattice) as shown in Figure 9.

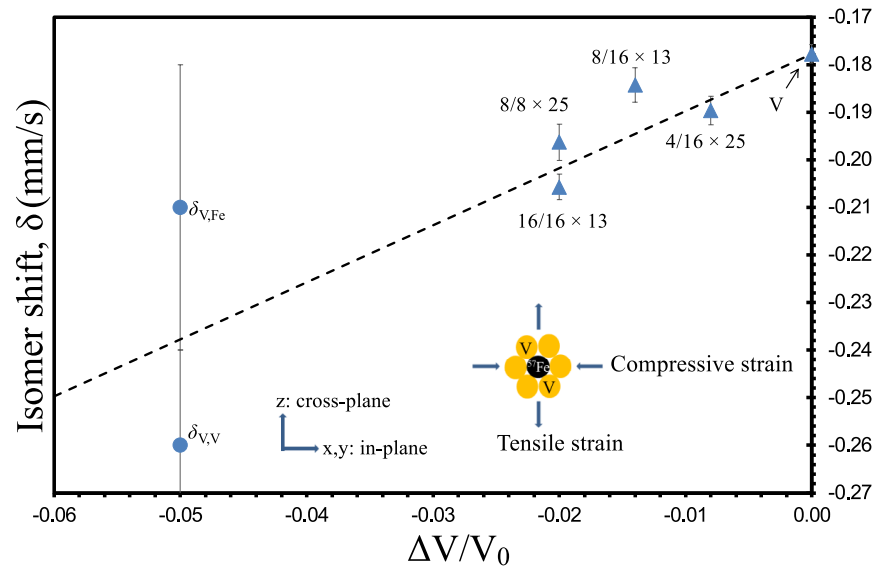


**Figure 9.** Plot of the isomer shift of the Fe atoms in pure vanadium foil as a function of the volume compression ( $\Delta V/V_0$ ) adapted with permission from [34] as compared to the measured isomer shifts of the  $Fe_V$  component ( $\delta_{Fe_V}$ ) from our work. Blue triangles are the measured  $\delta_{Fe_V}$  values from the Fe/V superlattice and pure V-layer as indicated. Dashed line is defined by  $\Delta\delta/\Delta(V/V_0) = 1.2$  mm/s adapted with permission from [34]. Copyrighted by the American Physical Society. The blue dots are the estimated isomer shifts for the 8/8 × 25 sample by Equations (4) ( $\delta_{V,Fe}$ ) and (5) ( $\delta_{V,V}$ ), respectively. A negative  $\Delta V/V_0$  indicates a compression and a positive  $\Delta V/V_0$  an expansion (tensile strain) of the V-lattice layer.

Figure 9 compares the observed isomer shift of the  $Fe_V$  component ( $\delta_{Fe_V}$ ) measured by eMS with the literature data obtained from the pure vanadium metal under high pressure reported by Ingalls et al. [34]. In the plot, the reported  $\delta_{Fe_V}$  value on the dashed line should match the measured  $\delta_{Fe_V}$  value from our superlattice sample where the  $^{57}Fe^+$  probe atoms could experience a maximum 5% in-plane compressive strain from the neighbouring V-lattices. As shown in Figure 9, for both the Fe/V superlattices and the pure V-layer, the data seem to follow the same trend as described by the dashed line despite that the neighbour effects at the interfaces were not considered in [34]. An isomer shift of  $-0.178(2)$  mm/s was measured for the pure V-layer with eMS (see Table 1). This value agrees well with the literature data of  $\delta_{Fe_V} = -0.17$  mm/s [34] from the pure vanadium metal. This confirms that to assign the single peak to the substitutional Fe in V-layers ( $Fe_V$ ) in our eMS is reasonable. The isomer shift  $\sim -0.19$  mm/s is measured in the eMS for the 8/8 × 25 sample for the substitutional Fe in the V-layer. This approves the strain effects in the V-lattice planes on the isomer shift of the  $^{57}Fe^+$  probe atoms in the superlattice structure.

The results in Figures 8 and 9 demonstrate that the strain status of the superlattices can be detected by the isomer shifts measured with eMS.

Figure 10 shows the fitted additional Lorentzian broadening of the line-width of the  $Fe_V$  component in the eMS spectra versus the relative Fe content in the Fe/V superlattices,  $Fe/(Fe+V)$ . When the line-width of the  $Fe_V$  component is compared between the pure vanadium sample and the V-layer in the Fe/V superlattices, a tendency of increasing line width with the Fe content in the superlattice is observed. This also matches the trends shown in Figures 8 and 9, which indicates that the 8/8 × 25 superlattice is fully strained and the 16/16 × 13 superlattice is less strained.

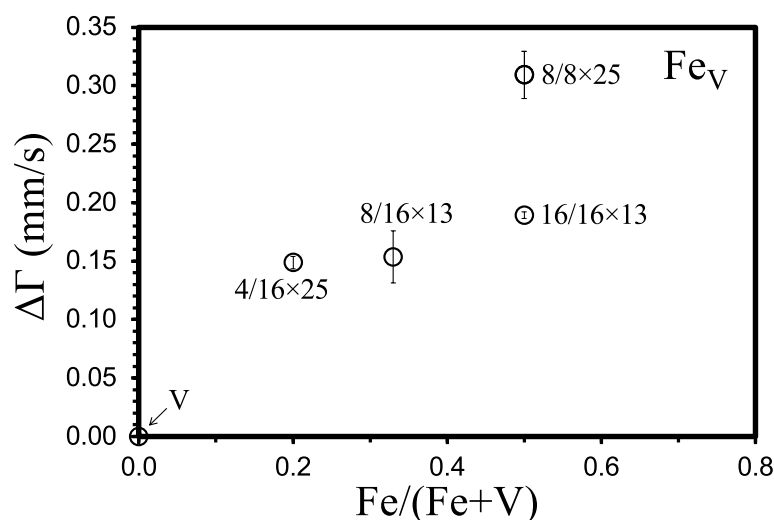


**Figure 10.** The additional Lorentzian broadening of the  $\text{Fe}_V$  spectral component in the eMS spectra from the pure V-layer and the Fe/V superlattices as indicated from Table 1.

Only a slightly broadened single line  $\text{Fe}_V$  component was observed in the eMS spectra of the superlattices in our study. This shows that there is no magnetic hyperfine field probed by the Fe atoms coming to rest in the V-layers in the superlattices at RT (see Table 1 and Figure 4). This agrees with the report [38] that no magnetic polarization of the V atoms was induced in the superlattices grown in the direction of V on Fe interfaces. This confirms that the broadening of the single line  $\text{Fe}_V$  component originated from the lattice strain in the V-layers.

## 5. Conclusions

We combine the CEMS with the on-line eMS following implantation of  $^{57}\text{Mn}^+$  to study the magnetic properties of the Fe/V superlattices and a pure V-layer at RT. The Fe/V superlattices and V-layers were epitaxially grown on MgO (100) substrates. The local lattice environment of the implanted  $^{57}\text{Fe}^+$  probes in the Fe-lattice layers, the V-lattice layers and at the Fe/V interfaces could be identified. The effect of the lattice strain on the isomer shifts and magnetic properties of the superlattices were confirmed by the eMS.

The eMS spectra of the superlattice appeared asymmetric and the isomer shift deviated from the bulk  $\alpha$ -Fe. This is due to the strain build-up in the superlattices. The effect of the strain on the isomer shift of the Fe-lattice layers in the superlattice structure agrees with the literature data for the pure Fe and vanadium samples under the high pressure.

Our work demonstrates that the combination of CEMS and eMS is a powerful tool to study the magnetism and lattice strain in the superlattices and multilayers at an atomic scale. Further works to explore the unique power of this technique at low temperatures to study samples patterned with lower dimensional 2D-magnetic structures are very interesting and feasible.

**Author Contributions:** Conceptualization, T.E.M., S.Ó., H.P.G. (Haraldur P. Gunnlaugsson) and B.Q.; methodology, T.E.M., S.Ó. and H.P.G. (Haraldur P. Gunnlaugsson); software, H.P.G. (Haraldur P. Gunnlaugsson); formal analysis, T.E.M. and H.P.G. (Haraldur P. Gunnlaugsson); resources, K.J.; investigation and data curation, T.E.M., S.Ó., H.P.G. (Haraldur P. Gunnlaugsson), R.M., H.M., K.B.-R., H.P.G. (Hafliði P. Gíslason), G.L., D.N. and G.W.; writing—original draft preparation, T.E.M., S.Ó., H.P.G. (Haraldur P. Gunnlaugsson) and B.Q.; writing—review and editing, B.Q., H.P.G. (Haraldur P. Gunnlaugsson), K.B.-R., R.M. and D.N.; supervision, S.Ó. and H.P.G. (Haraldur P. Gunnlaugsson); project administration, K.J.; funding acquisition, H.P.G. (Hafliði P. Gíslason) and K.B.-R. All authors have read and agreed to the published version of the manuscript.

**Funding:** The European Union Sixth Framework through RII3-EURONS; South African National Research Foundation; German BMBF (contract no. 05KK4TS1/9); Icelandic Research Fund.

**Data Availability Statement:** Data are available upon reasonable request.

**Acknowledgments:** Friðrik Magnus and Tryggvi K. Tryggvason for preparation of the superlattice samples.

**Conflicts of Interest:** The authors declare no conflict of interest.

## References

1. Gradmann, U. Magnetism in ultrathin transition metal films. In *Handbook of Magnetic Materials*; Buschow, K.H.J., Ed.; Elsevier: Amsterdam, The Netherlands, 1993; pp. 1–96.
2. Nakatani, R.; Hoshino, K.; Noguchi, S.; Sugita, Y. Magnetoresistance and Preferred Orientation in Fe–Mn/Ni–Fe/Cu/Ni–Fe Sandwiches with Various Buffer Layer Materials. *Jpn. J. Appl. Phys.* **1994**, *33*, 133–137. [[CrossRef](#)]
3. Granberg, P.; Isberg, P.; Svedberg, E.B.; Hjörvarsson, B.; Nordblad, P.; Wäppling, R. Antiferromagnetic coupling and giant magnetoresistance in Fe/V(0 0 1) superlattices. *J. Magn. Magn. Mater.* **1998**, *186*, 154. [[CrossRef](#)]
4. Kalska, B.; Häggström, L.; Blomquist, P.; Wäppling, R. Conversion electron Mössbauer spectroscopy studies of the magnetic moment distribution in Fe/V multilayers. *J. Phys. Condens. Matter* **2000**, *12*, 539–548. [[CrossRef](#)]
5. Nordstrom, E.; Kalska, B.; Haggstrom, L.; Blomqvist, P.; Wappling, R. Fe/V multilayers studied by CEMS. *J. Alloys Compd.* **2003**, *348*, 208–213. [[CrossRef](#)]
6. Magnuson, M. Induced magnetism at the interfaces of a Fe/V superlattice investigated by resonant magnetic x-ray scattering. *J. Magn. Magn. Mater.* **2017**, *422*, 362–366. [[CrossRef](#)]
7. Kamali, S. Mössbauer spectroscopy and its applications in spintronics. In *Nanomagnetism and Spintronics: Fabrication, Materials, Characterization and Applications*; Nasirpouri, F., Nogaret, A., Eds.; World Scientific: Singapore, 2010; p. 284.
8. Shinjo, T.; Hosoito, N.; Kawaguchi, K.; Takada, T.; Endoh, Y. Magnetism of Iron Interface in Contact with Vanadium. *J. Phys. Colloques* **1984**, *85*, C5-361–365. [[CrossRef](#)]
9. Wong, H.K.; Yang, H.Q.; Hilliard, J.E.; Ketterson, J.B. Magnetic properties of V/Fe superlattices. *J. App. Phys.* **1985**, *57*, 3660. [[CrossRef](#)]
10. Hjörvarsson, B.; Dura, J.A.; Isberg, P.; Watanabe, T.; Udovic, T.J.; Andersson, G.; Majkrzak, C.F. Reversible Tuning of the Magnetic Exchange Coupling in Fe/V (001) Superlattices Using Hydrogen. *Phys. Rev. Lett.* **1997**, *79*, 901. [[CrossRef](#)]
11. Ahlberg, M.; Papaioannou, E.T.; Nowak, G.; Hjörvarsson, B. Temperature dependence of magnetic properties in weakly exchange coupled Fe/V superlattices. *J. Magn. Magn. Mater.* **2013**, *341*, 142–147. [[CrossRef](#)]
12. Kalska, B.; Häggström, L.; Blomquist, P.; Wäppling, R. A study of the different interfaces in Fe/V superlattices. *Europhys. Lett.* **2001**, *53*, 395. [[CrossRef](#)]
13. Khizriev, K.S. Magnetic ordering in a model of superlattice Fe/V with the negative interlayer exchange interaction. *Solid State Commun.* **2009**, *149*, 464–466. [[CrossRef](#)]
14. Balogh, J.; Bujdosó, L.; Kaptás, D.; Dézsi, I.; Nakanishi, A. Top and bottom interfaces in Fe-B multilayers investigated by Mössbauer Spectroscopy. *Phys. Rev. B* **2012**, *85*, 195429. [[CrossRef](#)]
15. Güttlich, J.P.; Bill, E.; Trautwein, A.X. *Mössbauer Spectroscopy and Transition Metal Chemistry: Fundamentals and Applications*, 2011th ed.; Springer: Berlin/Heidelberg, Germany, 2011; pp. 1–135.
16. Przybylski, M. Structure and magnetism of Fe mono- and multi-layer systems as seen by conversion electron Mössbauer spectroscopy at atomic scale. *Hyperfine Interact.* **1998**, *113*, 135. [[CrossRef](#)]
17. Majkrzak, C.F. Neutron scattering studies of magnetic thin films and multilayers. *Physica B* **1996**, *221*, 342–356. [[CrossRef](#)]
18. Zabel, H.; Siebrecht, R.; Schreyer, A. Neutron reflectometry on magnetic thin films. *Physica B* **1996**, *17–21*, 276–278. [[CrossRef](#)]
19. Du, J.L.; Zhang, L.Y.; Fu, E.G.; Ding, X.; Yu, K.Y.; Wang, Y.G.; Wang, Y.Q.; Baldwin, J.K.; Wang, X.J.; Xu, P. Comparison of interface structure of BCC metallic (Fe, V and Nb) films on MgO (100) substrate. *App. Sur. Sci.* **2017**, *410*, 585–592. [[CrossRef](#)]
20. Fedoseyev, V.N.; Bätzner, K.; Catherall, R.; Evens, A.H.M.; Forkel-Wirth, D.; Jonsson, O.C.; Kugler, E.; Lettry, J.; Mishin, V.I.; Ravn, H.L.; et al. Chemically selective laser ion source of manganese. *Nucl. Instr. Meth. B* **1997**, *88*, 126. [[CrossRef](#)]
21. Weyer, G. Applications of parallel-plate avalanche counters in Mössbauer spectroscopy. In *Proceedings of Mössbauer Effect Methodology*; Springer: Boston, MA, USA, 1976.
22. Gunnlaugsson, H.P. A simple model to extract hyperfine interaction distributions from Mössbauer spectra. *Hyperfine Interact.* **2006**, *167*, 851. [[CrossRef](#)]
23. Isberg, P.; Hjörvarsson, B.; Wäppling, R.; Svedberg, E.B.; Hultman, H. Growth of epitaxial Fe/V (001) superlattice films. *Vacuum* **1997**, *48*, 483–489. [[CrossRef](#)]
24. Stevens, J.G. Isomer shift reference scales. *Hyperfine Interact.* **1983**, *13*, 221–236. [[CrossRef](#)]
25. Ziegler, J.F.; Ziegler, M.D.; Biersack, J.P. SRIM—The stopping and range of ions in matter. *Nucl. Instrum. Methods Phys. Res. Sect. B Beam Interact. Mater. Atoms* **2010**, *1818*, 268.
26. Li, X.Q.; Zhang, H.L.; Lu, S.; Li, W.; Zhao, J.J.; Johansson, B.; Vitos, L. Elastic properties of vanadium-based alloys from first-principles theory. *Phys. Rev. B* **2012**, *86*, 014105. [[CrossRef](#)]
27. Nirmala Louis, C.; Iyakutti, K. Electronic phase transition and superconductivity of vanadium under high pressure. *Phys. Rev. B* **2003**, *67*, 094509. [[CrossRef](#)]
28. Kittel, C. *Introduction to Solid State Physics*, 8th ed.; John Wiley & Sons: New York, NY, USA, 2015; p. 680.

29. Chen, Y.-L.; Yang, D.-P. *Mössbauer Effect in Lattice Dynamics: Experimental Techniques and Applications*; Wiley-VCH Verlag: Weinheim, Germany, 2007; p. 427.
30. Krause, J.C.; Schaf, J.; da Costa, M.I., Jr; Paduani, C. Effect of composition and short-range order on the magnetic moments of Fe in  $Fe_{1-x}V_x$  alloys. *Phys. Rev. B* **2000**, *61*, 6196–6204. [[CrossRef](#)]
31. Kopcewicz, M.; Jagielski, J.; Stobiecki, T.; Stobi, F. Ion-beam mixing and solid-state reaction of Fe-Zr multilayers. *J. Appl. Phys.* **1993**, *74*, 4363. [[CrossRef](#)]
32. Kopcewicz, M.; Jagielski, J.; Stobiecki, T.; Stobiecki, F.; Gawlik, G. Mössbauer study of ion-beam mixing of Fe/Zr multilayers. *J. Appl. Phys.* **1994**, *76*, 5232. [[CrossRef](#)]
33. Hindawi Publishing Corporation. Available online: <https://www.hindawi.com/journals/jnm/2013/959738/> (accessed on 7 June 2022).
34. Ingalls, R.; Drickamer, H.G.; de Pasquali, G. Isomer Shift of  $Fe^{57}$  in Transition Metals under Pressure. *Phys. Rev.* **1967**, *155*, 165. [[CrossRef](#)]
35. Southwell, W.H.; Decker, D.L.; Vanfleet, H.B. Mössbauer-Effect Measurements in Iron at High Pressures. *Phys. Rev.* **1968**, *171*, 354. [[CrossRef](#)]
36. Pipkorn, D.N.; Edge, C.K.; Debrunner, P.; De Pasquali, G.; Drickamer, H.G.; Frauenfeld, H. Mössbauer Effect in Iron under Very High Pressure. *Phys. Rev.* **1964**, *135*, A1604. [[CrossRef](#)]
37. Birch, J.; Sundgren, J.E.; Fewster, P.F. Measurement of the lattice parameters in the individual layers of single-crystal superlattices. *J. Appl. Phys.* **1995**, *72*, 6562. [[CrossRef](#)]
38. Uzdin, V.M.; Häggström, L. Atomic-scale magnetic and chemical structure of Fe/V multilayers using Mössbauer Spectroscopy. *Phys. Rev. B* **2005**, *72*, 024407. [[CrossRef](#)]